Simulation of Temperature Field Distribution in Melting TiAl Alloy by PAM Process

Xia Xu, Hui Chang, Hongchao Kou, Zhao Yang, Jinshan Li

***Abstract*—In this paper, the distribution of melt temperature field during Plasma Arc Cold Hearth Melting (PAM) process in TiAl alloy is investigated by computational simulation using the software FLUENT, and the effects of buoyancy, surface tension and process parameters on the melt temperature distribution of TiAl alloy in the second refining hearth were studied. The results show that the buoyancy and the surface tensions strongly affected the melingt temperature field distribution and they are the main cause to drive the fluid flow, thus the chemical composition uniformity of the melt can be improved through controlling the temperature field. The temperature increases as the power of the plasma gun is increased. Adjusting torch moving pattern and scanning frequency can be used to change the distribution of temperature field by controlling the residence time and the overheat of the melt.**

***Index Terms*—Melt temperature field distribution, PAM, Scanning frequency, Torch moving pattern.**

I. INTRODUCTION

TiAl alloy is one of the important high-temperature structural materials used in key parts of aeroengines and aircrafts for its advantages of low density, high specific strength, good oxidation resistance, corrosion resistance and high-temperature creep resistance, etc. Plasma Arc Cold Hearth Melting (PAM) process has a good control of the plasma torch energy flux which provides sufficient overheat of the alloy melt, and control of the residence time for inclusion particles in the water-cooled hearth, so it can effectively remove the high and low density inclusions by dissolution or mushy-zone entrapment [1-2]. The PAM furnace is filled with inert gas which can reduce volatilization of the high-saturation-vapor-pressure elements such as aluminum and chromium compared with VAR and EBM furnace, so the chemical composition of ingots can be easily controlled [3-4]. Therefore, the PAM technology is considered as the best one of the choices for preparing the large-size, high purity TiAl alloy ingot in recent years. The temperature field distribution during the PAM process remarkably impacts the melt physical properties, such as density, viscosity, elements diffusion coefficient, which related to the uniformity of alloy composition, removal of inclusion particles and ingot solidification behaviors [2-5]. So, in order to improve the quality of TiAl alloy ingot, it is necessary to study the temperature field distribution of the molten alloy during PAM process.

Taking into account of the too high temperature of plasma arc [6] to accurately measure the molten pool surface temperature by using traditional thermometer device, the computational simulation works are carried out to study the melt behaviors in the refining hearth by the 3D finite volume element software FLUENT to provide a pointer to the optimum operation of the PAM process.

Manuscript received on May, 2013.

Xia Xu, State Key Laboratory of Solidification Processing, Northwestern Polytechnical University, Xi'an 710072, P. R. China.

Assoc.Prof. Hui Chang, State Key Laboratory of Solidification Processing, Northwestern Polytechnical University, Xi'an 710072, P. R. China.

Assoc.Prof. Hongchao Kou, State Key Laboratory of Solidification Processing, Northwestern Polytechnical University, Xi'an 710072, P. R. China.

Zhao Yang, Research Institute, Baosteel Group Corporation, Shanghai 200940, P. R. China.

Prof. Jinshan Li, State Key Laboratory of Solidification Processing, Northwestern Polytechnical University, Xi'an 710072, P. R. China.

II. MODEL DESCRIPTION

A. Physical model

A 3300kW power PAM furnace equipped in Baosteel Special Materials Co., Ltd. is took as an example to studied, and the PAM process is shown schematically in Fig. 1. In this paper, the behavior of the melt in the second refining hearth is discussed, and the physical model of the melt is established as Fig. 2. As shown in Fig. 1, the molten metal flows into the water-cooled hearth through the inlet surface and flows over the outlet lip into a water-cooled copper mold to form ingot. The parameters of calculation model are designed as in Table I. In the PAM process, the plasma torch moves along a certain path through the moving torch operation. In the simulation, path of the plasma torch dynamically heating melt is shown in Fig. 3. The plasma torch moves back and forth along the straight-line AC with a cycle time of 4 seconds.

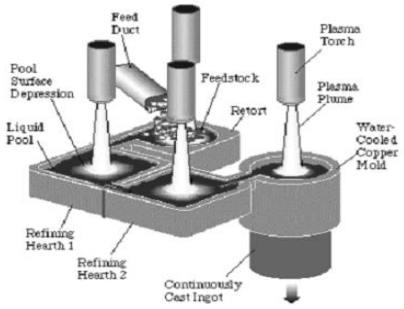

Fig.1 Schematic representation of the PAM process [1]

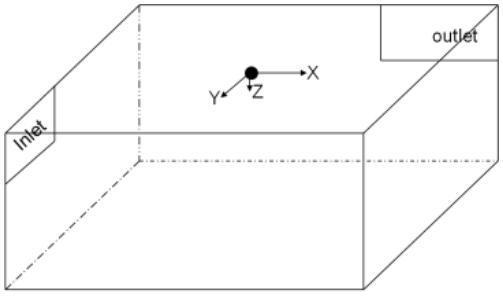

Fig.2 Model of the melt in the second refining hearth

Published By:
Blue Eyes Intelligence Engineering
& Sciences Publication

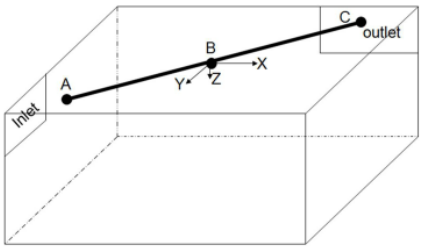

Fig.3 Plasma torch moving pattern

Table I Parameters of calculation model

Parameter		Value
Refining hearth	length	0.7m
	width	0.7m
	depth	0.3m
Inlet	length	0.3m
	depth	0.09m
Outlet	length	0.3m
	depth	0.09m

B. Mathematical model

According to above physical model and hydrodynamics theory, a transient mathematical model of the melt during plasma torch dynamically heating in the PAM process is obtained. In order to simplify calculation, assumptions are as follows: (1) thermal buoyancy effects is approximated by the Boussinesq hypothesis, which treats density as a constant value in all solved equations; (2) solidified region (mushy zone) maintains local thermodynamic equilibrium; (3) liquid-solid mushy zone is treated as a porous zone.

The melt flow, heat transfer, and solidification in the hearth region were computed by solving the 3-D incompressible mass equation, momentum equation, and energy conservation equation as followings:

Mass continuity equation

$$\nabla \cdot (\rho \vec{v}) = 0 \quad (1)$$

Momentum conservation equation

$$\frac{\partial}{\partial t}(\rho \vec{v}) + \nabla \cdot (\rho \vec{v}\vec{v}) = -\nabla p + \rho \vec{g} + \vec{F} \quad (2)$$

Energy conservation equation

$$\rho C_p \left(\frac{\partial T}{\partial t} + (\vec{v} \cdot \nabla)T\right) = \nabla \cdot k \nabla T + \rho L \frac{\partial f_s}{\partial t} + H \quad (3)$$

Where, ρ (kg/m^3) is mass density of the molten alloy, $\vec{v}$ (m/s) is fluid velocity, t (s) is time, p (Pa)is the static pressure, $\rho \vec{g}$ (N) is the gravity, $\vec{F}$ (N) is the external body forces, C_p (J·kg^{-1}·K^{-1}) is specific heat at constant pressure; T (K) is temperature; k (W·m^{-1}·K^{-1}) is thermal conductivity; L (J/kg) is latent heat of fusion; f_s is solid fraction in mushy zone, H (J) is the external body heat source terms.

C. Boundary conditions

1. Energy boundary conditions

Fourier condition is used in the model to express the heat transfer between the solidified metal and the water-cooled hearth walls. The heat-transfer coefficient takes into account the conductions of heat loss between metal and hearth.

At the surface of molten pool, the heat-transfer coefficient takes into account the combine of heat loss due to convection with plasma gas flow and radiation with ambient temperature. In addition, it is needed to consider the energy provided by the plasma torch. Gaussian flux profile [7-9] is assumed to describe the distribution of heat at the plasma impingment area and given by

$$q(r) = \frac{k}{\pi} * \eta * P * \exp(-kr^2) \quad (4)$$

Where, k is the power distribution factor; the greater of the k, the smaller of the heating area is and the more concentrated of the heat flux distribution is; r (m) is the distance from the center of the plasma impinging location; η is the power transfer efficiency; P (W) is the plasma torch power. Taking into account the feature of FLUENT, it is needed to input body heat source terms instead of heat flux density [9].

2. Momentum boundary conditions

At the inlet, mass flow rate has been set as the boundary. At the outlet, outflow has been set as boundary and one atmospheric pressure has been set for the ambient conditions.

3. Forces influencing the melt flow

The main forces influencing the melt flow are gravity, buoyancy, and surface tension, Darcy force and plasma impinging force [1, 7, 10-11].

3.1 Buoyancy

Buoyancy drives the natural-convection flows. The buoyancy term in the momentum equation is given by

$$F_b = \rho g \beta_T (T - T_0) \quad (5)$$

$$\beta_T = -\frac{1}{\rho}\left(\frac{\partial \rho}{\partial T}\right)_P \quad (6)$$

Where, ρ (kg/m^3) is the (constant) density of the molten alloy; β_T (K^{-1}) is the thermal expansion coefficient; T_0 (K) is the operating temperature.

3.2 Surface tension

Surface tension varies with the melt temperature, local surface tension gradients in the molten pool give rise to shear stresses. The shear stress (Marangoni effect) is given by

$$\tau = \frac{d\sigma}{dT} \cdot \nabla_s T \quad (7)$$

Where, $d\sigma/dT$ (N·m^{-1}·K^{-1}) is the surface tension gradient with respect to temperature, and $\nabla_s T$ is the surface gradient. This shear stress term is applied to the momentum equation.

3.3 Darcy force

An enthalpy-porosity technique [11] is used for modeling the solidification/melting process. It treats the mushy region (partially solidified region) as a porous medium. The porosity in each cell is set equal to the liquid fraction in that cell. In fully solidified regions, the porosity is equal to zero, which extinguishes the velocities in these regions. The momentum sink due to the reduced porosity in the mushy zone takes the following form:

$$S_D = \frac{(1-\beta)^2}{(\beta^3+\varepsilon)} A_{mush} \vec{v} \quad (8)$$

Where, β is the liquid volume fraction and it can be defined as (9); ε is a small number (0.001) to prevent division by zero; A_{mush} is the mushy zone constant, it measures the amplitude of the damping; the higher this value, the steeper the transition of the velocity of the material to zero as it solidifies; $\vec{v}$ is the fluid velocity in mushy zone.

$$\begin{aligned} &\beta = 0 \quad T<Ts \\ &\beta = 1 \quad T>Tl \\ &\beta = \frac{T-T_s}{T_l-T_s} \quad Ts<T<Tl \end{aligned} \quad (9)$$

Where, T is the melt temperature, T_l、T_s are the solidus and liquidus temperature, respectively.

3.4 Plasma impinging force

Plasma arc has a stirring effect on the molten bath under the self-inductance Lorentz force during the melting process.

Study found that the stirring effect of plasma torch is relatively weak [12], so it is not considered in this model.
An impinging plasma jet containing plasma flow and non-ionization inert gas stream give rise to a positive pressure and shear forces on the molten pool surface. The plasma impinging force is not considered in this paper.

D.Material parameters

The thermophysical properties of the materials (specific heat, thermal conductivity, thermal expansion coefficient and so on) usually vary with temperature, but they can be treated as an average value while the temperature changes in a small range. In this simulation, Ti-48Al-2Cr-2Nb alloy is selected and the physical properties of Ti-48Al-2Cr-2Nb alloy in the present calculations are shown in Table II.

Table II Physical properties of Ti-48Al-2Cr-2Nb [7]

Physical Constants	Value
Density ρ, kg/m^3	3636
Thermal expansion coefficient β_T, K^{-1}	10^{-4}
Thermal conductivity k, W/(m·K)	11.0
Latent heat of fusion ΔH, J/kg	3.77×10^5
Specific heat C_P, J/(kg·K)	727
Viscosity μ, kg/(m·s)	3.6×10^{-3}
Solidus temperature, K	1764
Liquidus temperature, K	1785

III. RESULTS AND DISCUSSIONS

A. Effect of buoyancy and surface tension on the melt temperature distribution

The process parameters are shown in Table III. At the moment that the plasma impinging location centre is located at point B (Fig. 3), the calculated temperature field on the molten pool surface and the skull profiles in the second refining hearth are shown in Fig. 4. Regardless of buoyancy and surface tension, the calculated temperature field on the molten pool surface is shown in Fig. 5.
Surface view of temperature contours show that the melt temperature rise with the heating effect of the plasma torch, and especially the temperature in the scanning area increases quickly. Comparing Fig. 5 with Fig. 4 (a), it is found that the melt in plasma heating area overheats seriously when considering no buoyancy and surface tension, and the overheat can be up to 300 K; when considering buoyancy and surface tension, the overheat is about 100 K. This phenomenon can be explained by the melt flow behavior influenced by buoyancy and surface tension.
Fig.6 shows the distribution of velocity vectors on selected planes in the refining hearth. Fig. 6 (a) and Fig. 6 (b) respectively represent the flowing behavior of the fluid on the molten pool surface and in the molten pool depth direction. As can be seen in Fig. 6 (a), the melt flows outwards the hearth walls from the torch impinging location center, and in Fig. 6 (b), the melt flows along two opposite convection-circle in the pool depth direction. Based on the analysis of the forces influencing the melt flow, we conclude that it is surface tension driving the melt flows from the hot region to the cold region at the free surface and it is buoyancy driving the high temperature melt flows upward and the low temperature melt sinks along the pool depth direction finally forming a circular flow.

Table III Processing parameters for the refining process

Parameter	Value
Torch power, kW	750
Torch moving pattern	Fig. 3
Torch scanning frequency, hz	0.25
Melting rate, kg/h	300

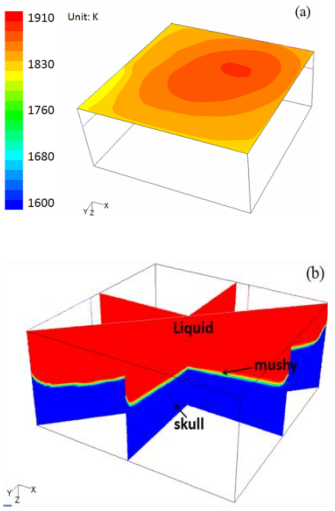

Fig. 4 Surface view of temperature contours (a) and skull profiles in the pool (b)

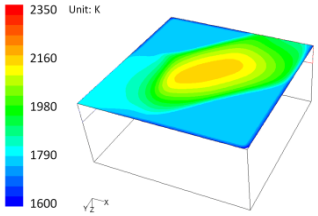

Fig. 5 Surface view of temperature contours considering no buoyancy and surface tension

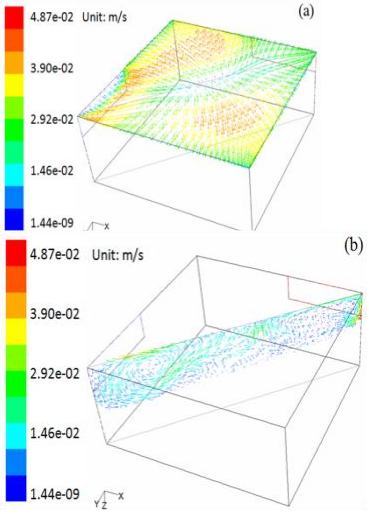

Fig. 6 Velocity vectors in the refining hearth

The results are shown in Fig. 4, Fig. 5 and Fig. 6: under the role of buoyancy and surface tension, the melt convective

Published By:
Blue Eyes Intelligence Engineering
& Sciences Publication

flows and mixes and the flowing behavior helps to reduce the melt overheat.

B. Effect of plasma torch power on the melt temperature distribution

The effect of plasma torch power on the temperature distribution at the molten pool surface is discussed as follows. In the simulation, the melting rate is 300 kg/h, the torch moving pattern is shown in Fig.3 and the plasma torch power changes from 650 kW to 750 kW. When the plasma impinging location centre is located at point B, the predicted temperature distribution on AC line at free surface is shown in Fig. 7.

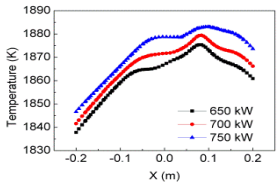

Fig.7 Relationship between temperature on pool surface and torch power

As shown in Fig. 7, the melt temperature rises differently due to the change of torch power. The thermal equilibrium of the refining system can be expressed as Q=Cp×m×△T+Qloss, where Q is the energy provided by the plasma torch whose power value is P, m is the melt mass in the hearth, Cp is the specific heat, △T is the amount of temperature variation, Qloss is the heat loss due to radiation and convection and conduction heat transfer between melt and hearth walls or ambient enviroment. When the melting rate is constant, m is determined and Qloss changes little, so △T will largen when increasing the Q. It is can be said that the greater the torch power, the higher the melt temperature will be.

C. Effect of plasma torch scanning frequency on the melt temperature distribution

The effect of plasma torch scanning frequency on the temperature distribution at the molten pool surface is discussed as follows. In the simulation, the plasma torch power is 750 kW, the melting rate is 300 kg/h, the torch moving pattern is shown in Fig.3 and the plasma torch scanning frequency changes from 0.0833 hz to 0.5 hz. When the plasma impinging location centre is located at point B, the predicted temperature distribution on AC line at free surface is shown in Fig. 8.

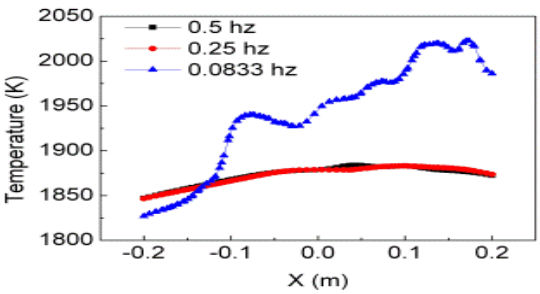

Fig.8 Relationship between temperature on pool surface and scanning frequency

As shown in Fig.8, the melt temperature rises differently when the plasma torch takes different scanning frequency. When the scanning frequency is 0.0833 hz, the melt maximum temperature reaches 2022.83 K, the temperature distribution and the skull profiles at the pool surface are shown in Fig. 9. When the scanning frequency is 0.25 hz, the melt maximum temperature reaches 1883.09 K and the temperature distribution of the melt at the pool surface is shown in Fig. 4(a). . When the scanning frequency is 0.5 hz, the melt maximum temperature reaches 1884.01 K and the temperature distribution is little different with that when the scanning frequency is 0.25 hz.

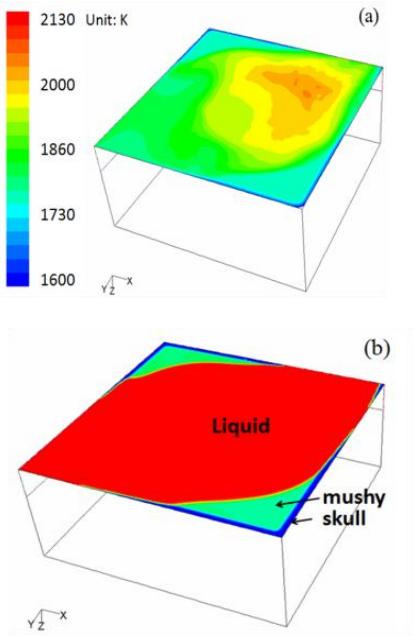

Fig. 9 Surface view of temperature contours (a) and skull profiles (b) in the pool

Fig. 9 shows the melt in the plasma torch scanning location overheats seriously. Comparing with the situation when the scanning frequency is 0.25 hz, the melt temperature gradients are larger when the scanning frequency is 0.0833 hz. It can be concluded that adjusting the torch scanning frequency can change the temperature distribution of the melt in the torch scanning location in the case of the torch power and melting rate are constant. In this simulation, the result shows that the melt temperature is higher when the scanning frequency is 0.0833 hz than the other two case.

D.Effect of plasma torch moving pattern on the melt temperature distribution

In the simulation, two moving patterns of linear and triangular shaped are discussed. The linear moving pattern is shown in Fig. 3 and the triangular moving pattern is shown in Fig. 10. As shown in Fig. 10, the plasma torch shifts along the path of the straight-line AB, BC and CA.

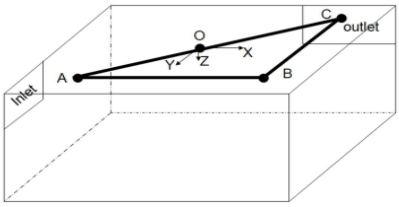

Fig. 10 Triangular shaped torch moving pattern

When the plasma torch power is 750 kW, the melting rate is 300 kg/h, the plasma torch scanning frequency is 0.25 hz and the plasma impinging location centre is located at point O, the predicted temperature distribution on AC line at free surface are shown in Fig. 4(a) about linear pattern and Fig. 11(a) about triangular pattern.

As shown in Fig. 4(a) and Fig. 11(a), the melt is heated differently when the plasma torch takes different moving pattern. The difference mainly contains the amount of the melt temperature variation and the position of the melt where temperature is maximum.

Because of buoyancy and surface tension which drive the melt flow from the hot region to the cold region and the difference of the temperature fields as shown in Fig. 4(a) and Fig. 11(a), it is different about the melt flowing behavior as shown in Fig. 6(a) and Fig. 11(b). From Fig. 6(a), it can be seen that the melt flows toward the outlet lip along the path of vector segment AC (Fig. 3), and From Fig. 11(b), the melt flows successively toward the outlet lip along the path of vector segment AB and BC. In this simulation, the result shows that the time of the melt flowing through the refining hearth when the plasma torch movement takes triangular pattern is longer than that case of taking linear pattern.

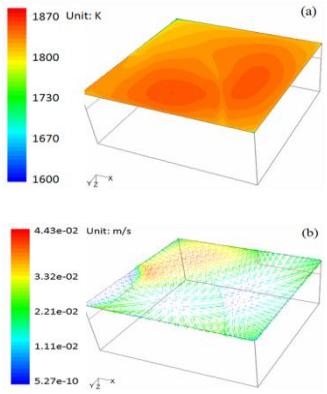

Fig. 11 Surface view of temperature contours (a) and velocity vector (b) in the pool

IV. CONCLUSIONS

A model for numerical calculation of the melt temperature distribution during refining Ti-48Al-2Cr-2Nb alloy in the PAM process was presented. Based on the model, the influence of buoyancy, surface tension and process on the temperature distribution of the melt in the second refining hearth has been simulated and analyzed.

Simulation results show that buoyancy and surface tension drive the melt flow and mix, the flowing behavior helps to reduce the melt overheat and homogenize the melt composition.

Simulation results also show that the influence of torch power, scanning frequency and moving pattern on the melt temperature is significant. The larger the torch power, the higher the melt temperature is. The torch scanning frequency can be used to control the local melt temperature. The melt temperature rises more significantly when the torch scanning frequency is 0.0833hz than the other two cases. The torch moving pattern can be used to control the residence time of the melt in the refining hearth. The residence time is longer when the plasma torch movement takes triangular pattern than that when taking linear pattern.

ACKNOWLEDGMENT

This work was supported by National Basic Research Program of China (973 Project) (No. 2011CB605502).

REFERENCES

1. S.V. Patankar, “Computational modeling of flow and heat transfer in industrial applications,” International Journal of Heat and Fluid Flow, vol. 23, no. 3, pp. 222-231, June 2002.
2. J.M. Cai, J.M. Ma, M.Y. Meng, Z.X. Li, C.X. Cao, “Hard Alpha Defect in Titanium Alloys and its Control Using Plasma Arc Cold Hearth Melting Technique,” Failure Analysis and Prevention, vol. 2, no.2, pp. 51-57, May 2007.
3. J.R. Wood, “Melting and casting of gamma titanium aluminide ingots,” Gamma Titanium Aluminides 2003, pp. 227-232, 2003, Gamma Titanium Aluminides 2003.
4. J.P. Bellot, E. Hess, and D. Ablitzer, “Aluminum volatilization and inclusion removal in the electron beam cold hearth melting of Ti alloys,” Metallurgical and Materials Transactions B: Process Metallurgy and Materials Processing Science, vol. 31, no. 4, pp. 845-854, Aug 2000.
5. H.V. Zhuk, P.A. Kobryn, and S.L. Seniatin, “Influence of heating and solidification conditions on the structure and surface quality of electron-beam melted Ti-6Al-4V ingots,” Journal of Materials Processing Technology, vol. 190, no. 1-3, pp. 387-392, July 2007.
6. S.C. Chu, S.S. Lian, “Numer ical analysis of temperature distribution of plasma arc with molten pool in plasma arc melting,” Computational Materials Science, vol. 30, no. 3-4, pp. 441-447, August 2004.
7. K.B. Bisen, M. Arenas, N. EI-Kaddah, V.L. Acoff, “Computation and validation of weld pool dimensions and temperature profiles for gamma TiAl,” Metallurgical and Materials Transactions A: Physical Metallurgy and Materials Science, vol. 34A, no. 10, pp. 2273-2279, October 2003.
8. R.H. Zhang, Seiji Katayama, Naitou Yasuaki, D. Fan, “Numerical simulation of the laser welding by using the Rotary-Gauss body heat source model,” Electric Welding Machine, vol. 37, no. 5, pp. 51-54, May 2003.
9. A. Powell, J. Van Den Avyle, B. Damkroger, J. Szekely, U. Pal, “Analysis of multicomponent evaporation in electron beam melting and refining of titanium alloys,” Metallurgical and Materials Transactions B: Process Metallurgy and Materials Processing Science, Vol. 28, no. 6, pp. 1227-1234, Dec 1997.
10. L. Ma, “The three dimensional numerical simulation of temperature and fluid Flow fields of plasma arc welding,” Tianjin University, pp. 11-21, 2006.
11. “Fluent 6.3 User’s Guide,” Fluent Inc., pp. 1793-1806, 2006.
12. Y.Y. Zhao, R.M. Ward, T.P. Johnson, “Numerical modeling of electromagnetic stirring of liquid pool in plasma arc melting,” Electromagnetic Processing of Materials, Proc of the International Congress on Electromagnetic Processing of Materials, May 1997.
13. Xia Xu, master degree candidate for Materials Science, mainly engaged in the studies of melting and refining TiAl alloy

AUTHORS PROFILE

Assoc.Prof. Hui Chang, Ph.D., State Key Laboratory of Solidification Processing, Northwestern Polytechnical University, China, Research Interests include Phase transformation on titanium alloy, Processing of titanium and titanium alloy, and Microstructure and properties of titanium alloy

Assoc.Prof. Hongchao Kou, Ph.D., State Key Laboratory of Solidification Processing, Northwestern Polytechnical University, China, Research Interests include Bulk Metallic Glasses and Titanium Alloy

Zhao Yang, lead researcher of the Research Institute, Baosteel Group Corporation, charge of manufacturing of titanium and titanium Alloy

Prof. Jinshan Li, Ph.D., vice director of the State Key Laboratory of Solidification Processing, Northwestern Polytechnical University, China, Research Interests include Electromagnetic Constraint Forming and Directional Solidification, High Gradient Directional Solidfication Continuous Casting, and Melt Treatment and Super thinning of Tissue.